



# Dual-wavelength-pumping of mid-infrared Tm:YLF laser at 2.3 $\mu\text{m}$ : demonstration of pump seeding and recycling processes

Hippolyte Dupont, Lauren Guillemot, Pavel Loiko, Alain Braud, Jean-Louis Doualan, Patrice Camy, Patrick Georges, Frédéric Druon

## ► To cite this version:

Hippolyte Dupont, Lauren Guillemot, Pavel Loiko, Alain Braud, Jean-Louis Doualan, et al.. Dual-wavelength-pumping of mid-infrared Tm:YLF laser at 2.3  $\mu\text{m}$ : demonstration of pump seeding and recycling processes. Optics Express, 2022, 30 (18), pp.32141. 10.1364/OE.468695 . hal-03798899

**HAL Id: hal-03798899**

**<https://hal-iogs.archives-ouvertes.fr/hal-03798899>**

Submitted on 5 Oct 2022

**HAL** is a multi-disciplinary open access archive for the deposit and dissemination of scientific research documents, whether they are published or not. The documents may come from teaching and research institutions in France or abroad, or from public or private research centers.

L'archive ouverte pluridisciplinaire **HAL**, est destinée au dépôt et à la diffusion de documents scientifiques de niveau recherche, publiés ou non, émanant des établissements d'enseignement et de recherche français ou étrangers, des laboratoires publics ou privés.

# Dual-wavelength-pumping of mid-infrared Tm:YLF laser at 2.3 $\mu\text{m}$ : demonstration of pump seeding and recycling processes

HIPPOLYTE DUPONT,<sup>1</sup> LAUREN GUILLEMOT,<sup>2</sup> PAVEL LOIKO,<sup>2</sup> ALAIN BRAUD,<sup>2</sup> JEAN-LOUIS DOUALAN,<sup>2</sup> PATRICE CAMY,<sup>2</sup> PATRICK GEORGES,<sup>1</sup> AND FRÉDÉRIC DRUON<sup>1,\*</sup>

<sup>1</sup>Université Paris-Saclay, Institut d'Optique Graduate School, CNRS, Laboratoire Charles Fabry, 91127 Palaiseau, France

<sup>2</sup>Centre de Recherche sur les Ions, les Matériaux et la Photonique (CIMAP), UMR 6252 CEA-CNRS-ENSICAEN, Université de Caen, 6 Boulevard Maréchal Juin, 14050 Caen Cedex 4, France

\*frederic.druon@institutoptique.fr

**Abstract:** Upconversion pumping of thulium lasers emitting around 2.3  $\mu\text{m}$  (the  $^3\text{H}_4 \rightarrow ^3\text{H}_5$  transition) has recently attracted a lot of attention as it is compatible with the mature Yb-laser technology. To explore this possibility, we built a mid-infrared Tm:LiYF<sub>4</sub> laser pumped by an Yb:CaF<sub>2</sub> laser at 1.05  $\mu\text{m}$  delivering an output power of 110 mW at 2.31  $\mu\text{m}$  for a maximum incident pump power of 2.0 W. A strong absorption issue appeared in the Tm laser: the slope efficiency vs. the incident pump power was 7.6% while that vs. the absorbed pump power reached 29%. To overcome this issue, a dual-wavelength pumping at 0.78  $\mu\text{m}$  and 1.05  $\mu\text{m}$  was explored (combining both the direct and upconversion pumping schemes). The reciprocal interplay between the two pumps was studied to evaluate their benefits in terms of the pump absorption and laser efficiency. We observed an interesting decrease of the laser threshold for upconversion pumping when adding a small fraction of the direct pump revealing a seeding effect for the excited-state absorption from the metastable  $^3\text{F}_4$  level. A recycling process of this manifold by excited-state absorption in the  $^3\text{F}_4 \rightarrow ^3\text{F}_{2,3}$  loop was also observed. The pump absorption seeding is a viable route for the development of low-threshold upconversion pumped thulium lasers.

© 2022 Optical Society of America under the terms of the [OSA Open Access Publishing Agreement](#)

## 1. Introduction

Mid-infrared (MIR) lasers emitting at the wavelengths around 2.3  $\mu\text{m}$  (falling into the 2.0–2.4  $\mu\text{m}$  atmospheric window, the K band) are of practical importance for spectroscopy of various atmospheric and biological species such as HF, CO, CH<sub>4</sub>, H<sub>2</sub>CO and C<sub>6</sub>H<sub>12</sub>O<sub>6</sub> leading to applications in the atmosphere gas sensing and pollutant detection, combustion studies and non-invasive glucose blood measurements [1,2]. Such laser sources are also interesting for pumping of mid-infrared optical parametric oscillators (OPOs) [3].

There exist several approaches to address this spectral range, namely by using lasers based on zinc chalcogenide crystals (ZnS, ZnSe) doped with Cr<sup>2+</sup> ions [4]; semiconductor (GaInAs / InP or GaInAsSb / GaSb) Vertical-Cavity Surface-Emitting Lasers (VCSELs) [5]; Raman-shifted pulsed Tm or Ho lasers with a fundamental emission at 2  $\mu\text{m}$  [6] or (iv) OPOs [3]. Finally, the thulium ions (Tm<sup>3+</sup>) themselves can provide a direct generation of the 2.3  $\mu\text{m}$  radiation [7,8] according to the  $^3\text{H}_4 \rightarrow ^3\text{H}_5$  electronic transition, Fig. 1(a). Note that Tm<sup>3+</sup> ions can be efficiently pumped at 0.78–0.8  $\mu\text{m}$  (directly to the  $^3\text{H}_4$  state) using commercial high-power AlGaAs laser diodes [9]. The main advantages of 2.3  $\mu\text{m}$  bulk Tm lasers are the developed growth technology of high optical quality Tm<sup>3+</sup>-doped fluoride and oxide crystals, the availability of cheap ; simple and high-power pump sources (e.g., fiber-coupled AlGaAs diode lasers and Yb fiber lasers, see below) ; direct laser emission at 2.2–2.4  $\mu\text{m}$  avoiding any

frequency conversion steps ; the possibility to operate both in the continuous-wave and pulsed regimes and high quality of the laser beam. In this way, Tm lasers operating on the  $^3H_4 \rightarrow ^3H_5$  transition may represent a simple and cheap alternative to  $Cr^{2+}$ -ion-based lasers at the expense of much narrower gain bandwidth. The emission range of such Tm lasers is also filling the gap between other direct emission of rare-earth-ions in the near-mid-IR, namely  $Ho^{3+}$  ( $^5I_7 \rightarrow ^5I_8$ ,  $\sim 2.1 \mu m$ ) and  $Er^{3+}$  ( $^4I_{11/2} \rightarrow ^4I_{13/2}$ ,  $\sim 2.8 \mu m$ ).

During the last years, a great progress in developing continuous-wave (CW) [10-14] and mode-locked (ML) [15,16] Tm lasers operating on the  $^3H_4 \rightarrow ^3H_5$  transition has been demonstrated using various (both fluoride and oxide) laser crystals. Guillemot *et al.* reported on a CW Tm:KY<sub>3</sub>F<sub>10</sub> laser directly pumped at  $0.78 \mu m$  and generating  $0.84 W$  at  $2.34 \mu m$  [12]. Loiko *et al.* showed that the slope efficiency of such a laser may exceed the Stokes limit owing to the efficient energy-transfer upconversion (ETU) process for adjacent Tm<sup>3+</sup> ions,  $^3F_4 + ^3F_4 \rightarrow ^3H_6 + ^3H_4$ , Fig. 1(a), refilling the upper laser manifold [10]. Souldard *et al.* reported on a SESAM ML Tm:LiYF<sub>4</sub> laser delivering  $94 ps$  pulses at  $2.31 \mu m$  [15]. Canbaz *et al.* achieved femtosecond pulses ( $514 fs$ ) from a similar laser using the Kerr-lens mode-locking technique [16]. Note that both ML lasers were pumped by a Ti:Sapphire laser at  $0.78 \mu m$ .

Later, alternative upconversion (UC) pumping schemes at  $1 \mu m$  and  $1.5 \mu m$  were proposed for such lasers [17,18]. Among them, the first one is more attractive as it is compatible with the mature Yb-bulk and Yb-fiber laser technologies. It is based on a weak (non-resonant) ground-state absorption (GSA) corresponding to the short-wave vibronic sideband of the  $^3H_6 \rightarrow ^3H_5$  Tm<sup>3+</sup> absorption band and a strong (resonant) excited-state absorption (ESA) from the metastable Tm<sup>3+</sup> state,  $^3F_4 \rightarrow ^3F_{2,3}$ , Fig. 1(a). The population of the intermediate level  $^3F_4$  is mainly provided by the photon avalanche effect [19] relying on both the above-mentioned resonant ESA channel and the well-known cross-relaxation (CR) process for Tm<sup>3+</sup> ions,  $^3H_4 + ^3H_6 \rightarrow ^3F_4 + ^3F_4$ . Note that due to the non-resonant nature of the GSA transition, the population of the  $^3F_4$  state via the non-radiative path from the short-living  $^3H_5$  state is almost negligible. The photon avalanche process recycles the populations of Tm<sup>3+</sup> multiplets in favor of the  $^3H_4$ , and  $^3F_4$  ones acting as the upper laser level and the “effective” ground-state, respectively. Tyazhev *et al.* reported on a watt-level Tm fluoride fiber laser generating  $1.24 W$  at  $2.28 \mu m$  with a slope efficiency of 37% based on a single-wavelength UC pumping at  $1.05 \mu m$  using an Yb-fiber laser [20].

So far, the main disadvantages of the UC pumping scheme for bulk MIR Tm lasers are the limited pump absorption and relatively high laser threshold. This is explained by the need of populating the intermediate  $^3F_4$  Tm<sup>3+</sup> state via the photon avalanche mechanism which becomes efficient only at high pump intensities. It would be attractive to combine both pump schemes (direct and UC pumping) to improve these performances. Wang *et al.* studied dual-wavelength pumping at  $0.79$  and  $1.47 \mu m$ : a diode-pumped Tm:LiYF<sub>4</sub> laser delivered  $1.8 W$  at  $2.31 \mu m$  for a total incident pump power of  $70 W$  [21]. Besides the low optical-to-optical efficiency of only 2.5%, the output power of the Tm laser saturated while increasing the pump power at  $1.47 \mu m$  and no lasing under single UC pumping was achieved. Thus, the potential of dual-wavelength pumping was not clearly revealed.

In the present work, we report on a mid-infrared thulium laser operating on the  $^3H_4 \rightarrow ^3H_5$  transition with a dual-wavelength (direct and upconversion) pumping at  $0.78$  and  $1.05 \mu m$  (i.e., relying on the Yb-laser technology). As a gain material, we have selected Tm<sup>3+</sup>-doped lithium yttrium fluoride crystal (LiYF<sub>4</sub>) which currently appears as a state-of-the-art material for this type of lasers.

## 2. Experimental

### 2.1 Spectroscopy of Tm:LiYF<sub>4</sub>: An overview

Prior to the laser experiments, let us briefly describe the relevant spectroscopic parameters of Tm<sup>3+</sup> ions in the LiYF<sub>4</sub> crystal. The stimulated-emission cross-section for the  $^3H_4 \rightarrow ^3H_5$

transition reaches  $\sigma_{SE} = 0.52 \times 10^{-20} \text{ cm}^2$  at 2303 nm for  $\pi$ -polarization, Fig. 1(b). The intrinsic lifetime of the upper laser level  $^3\text{H}_4$   $\tau_{lum,0} = 2.3 \text{ ms}$  and for 3.5 at.% Tm doping, the self-quenching via CR leads to a reduced value of  $\tau_{lum} \sim 155 \mu\text{s}$  [10]. For the  $^3\text{H}_6 \rightarrow ^3\text{H}_4$  GSA transition, the peak cross-section  $\sigma_{GSA} = 0.85 \times 10^{-20} \text{ cm}^2$  at 779.9 nm for  $\pi$ -polarization (bandwidth at FWHM: 7.6 nm), see Fig. 1(c). For the  $^3\text{F}_4 \rightarrow ^3\text{F}_{2,3}$  ESA transition, the peak cross-section  $\sigma_{ESA} = 0.63 \times 10^{-20} \text{ cm}^2$  at 1042.0 nm and at longer wavelengths, another less intense peak appears with  $\sigma_{ESA} = 0.32 \times 10^{-20} \text{ cm}^2$  at 1051.6 nm (for  $\sigma$ -polarization), Fig. 1(d). The FWHMs of these peaks are 2.5 nm and 4.3 nm, respectively. The  $^3\text{H}_6 \rightarrow ^3\text{H}_5$  GSA is weak between 1000 nm and 1100 nm ( $\sigma_{GSA} \approx 0.01 \times 10^{-20} \text{ cm}^2$  in this region) since it is located in the tail of the peak at 1.20  $\mu\text{m}$  (for  $\pi$ -polarization) that has a value of  $\sigma_{ESA} = 0.62 \times 10^{-20} \text{ cm}^2$ .

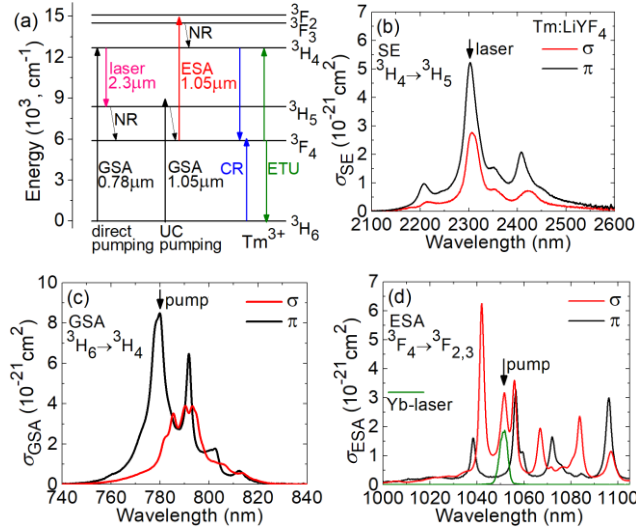


**Fig. 1.** (a) The scheme of energy levels of thulium ions relevant for MIR laser operation: GSA and ESA – ground- and excited-state absorption, respectively, NR – non-radiative relaxation, CR – cross-relaxation, ETU – energy-transfer upconversion; (b-d) Spectroscopy of Tm<sup>3+</sup> ions in LiYF<sub>4</sub>: (b) simulated-emission (SE) cross-sections,  $\sigma_{SE}$ , the  $^3\text{H}_4 \rightarrow ^3\text{H}_5$  transition; (c) GSA cross-sections,  $\sigma_{GSA}$ , the  $^3\text{H}_6 \rightarrow ^3\text{H}_4$  transition; (d) ESA cross-sections,  $\sigma_{ESA}$ , the  $^3\text{F}_4 \rightarrow ^3\text{F}_{2,3}$  transition. The light polarizations:  $\pi$  and  $\sigma$ . In (d), the spectrum of the Yb:CaF<sub>2</sub> laser is shown for comparison.

## 2.2 Laser set-up

The scheme of the dual-wavelength-pumped MIR thulium laser is shown in Fig. 2. As a gain medium, we use an  $\alpha$ -cut 3.5 at.% Tm:LiYF<sub>4</sub> crystal ( $\Phi=8.5 \text{ mm}$ , thickness=8.14 mm). Its faces are polished to laser-quality with good parallelism and left uncoated. The crystal is glued to a Cu-holder and it is passively cooled. A hemispherical laser cavity is composed of a flat pump mirror (PM) coated for high transmission (HT) at the pump wavelengths ( $T = 95\%$  at 1.05  $\mu\text{m}$  and 0.78  $\mu\text{m}$ ) and high reflection (HR,  $R > 99.9\%$ ) at 2.3  $\mu\text{m}$ , and a concave (radius of curvature: RoC = -100 mm) output coupler (OC) having a transmission at the laser wavelength  $T_{OC} = 2\%$ . The OC also provides HT at 1.9  $\mu\text{m}$  to suppress the laser on the  $^3\text{F}_4 \rightarrow ^3\text{H}_6$  transition. The geometrical cavity length is 99 mm.

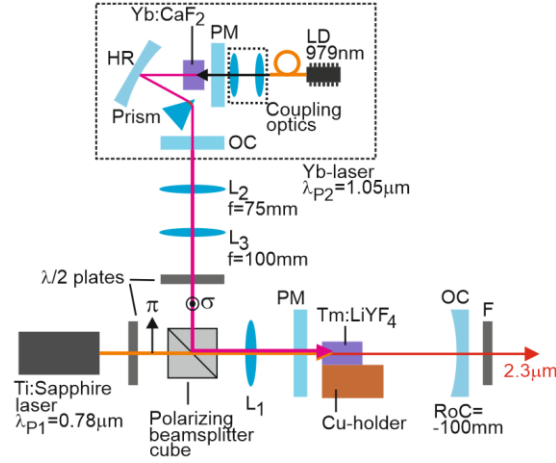


**Fig. 2.** Set-up of the dual-wavelength-pumped MIR thulium laser: PM – pump mirror, OC – output coupler, HR – highly-reflective mirror, L<sub>1</sub>, L<sub>2</sub>, L<sub>3</sub> – aspherical lenses, λ/2 – half-wave plates, LD – laser diode, F – band-pass filter.

Two pump sources are used. The first one addresses the  $^3H_6 \rightarrow ^3H_4$  GSA transition (the direct pumping). It is a Ti:Sapphire laser (Spectra Physics, model 3900J) delivering up to 3.0 W at  $\lambda_{P,GSA} = 780$  nm (linewidth at FWHM: 0.1 nm) with a beam quality factor  $M^2 \approx 1$  and a linear polarization aligned to correspond to  $\pi$  in the Tm-crystal. Its output is focused into the laser crystal using a lens (L<sub>1</sub>). Several L<sub>1</sub> focusing lenses with a focal length in the range of 50 – 150 mm are tested. For  $f = 150$  mm (the optimum one for single wavelength pumping at  $\lambda_{P,GSA} = 0.78 \mu\text{m}$ ), the measured pump beam waist  $2w_P$  is  $61 \pm 5 \mu\text{m}$ .

The second pump source is designed to address the  $^3F_4 \rightarrow ^3F_{2,3}$  ESA transition (the UC pumping scheme). A home-made tunable Ytterbium-bulk laser is based on a 2 at.% Yb:CaF<sub>2</sub> crystal pumped by a fiber-coupled InGaAs laser diode at 979 nm. A V-shaped laser cavity is composed of a flat pump mirror, a concave (RoC = -200 mm) HR mirror and a plane OC ( $T_{OC} = 5\%$ ). The wavelength tuning is realized by inserting an SF10 prism close to the OC. The maximum of the output power of the tunable Yb:CaF<sub>2</sub> laser is observed at  $\sim 1.05 \mu\text{m}$ , thus, we select the thulium ESA peak at 1051.6 nm for UC pumping, cf. Fig. 1(b), even though another ESA peak at 1042.0 nm is more intense. The tunable Yb-laser delivers up to 1 W at  $\lambda_{P,UC} = 1050$  nm (linewidth:  $\sim 3$  nm) with a linear polarization corresponding to  $\sigma$  in the Tm-crystal. Without the prism, in the free-running regime, the Yb-laser can be scaled up to 2 W (after the polarizer Fig. 2) at a central wavelength of 1050 nm. The size of the pump beam from the Yb-laser is adjusted using an afocal telescope system composed of two lenses (L<sub>2</sub>:  $f = 75$  mm, L<sub>3</sub>:  $f = 100$  mm) and the polarization state – using a half-wave plate. For this pump source, the measured pump spot size in the crystal  $2w_P$  is  $30 \pm 5 \mu\text{m}$  (for L<sub>1</sub> lens with a focal length of  $f = 50$  mm, being the optimum one for pure UC pumping). The two pump beams are combined using a polarizing beam-splitter cube (Thorlabs PBS252). The pumping is in double-pass because of the partial reflectivity of the OC at the pump wavelengths ( $R_{0.78\mu\text{m}} = 64\%$  and  $R_{1.05\mu\text{m}} = 28\%$ ). The residual (non-absorbed) pump after the OC is filtered out using a band-pass filter (Thorlabs, FB2250-50).

### 3. Results and discussion

The wavelength of the Yb:CaF<sub>2</sub> laser is continuously tuned from 1032 to 1054 nm, Fig. 3(a). To justify the selection of the pump wavelength, we have studied the single-pass pump absorption as a function of  $\lambda_{P,UC}$  and the incident pump power, Fig. 3(b). The highest pump absorption is observed at 1050 nm in agreement with the ESA spectra of Tm<sup>3+</sup> ions in LiYF<sub>4</sub> for  $\sigma$ -polarization, cf. Fig. 1(d). A certain pump level is needed to reach a kind of plateau for

pump absorption (~30%). Thus, tuning the pump wavelength to match precisely one of the ESA peaks is indeed critical as otherwise we are not able to reach reasonably high pump absorption even for high pump levels.

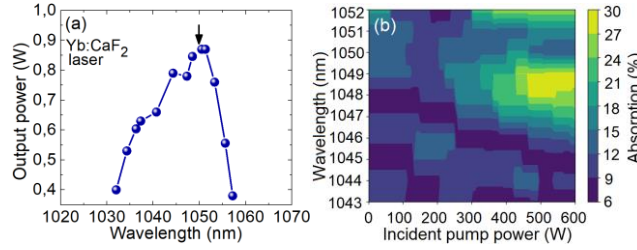


**Fig. 3.** (a) Wavelength tuning curve of the Yb:CaF<sub>2</sub> laser, *arrow* – the selected laser wavelength; (b) A 2D plot of single-pass pump absorption in the Tm:LiYF<sub>4</sub> crystal (σ-polarized pump) vs. the pump wavelength and the incident pump power.

Due to the different physical processes involved in the pump absorption between the cases of direct pumping (the GSA  $^3\text{H}_6 \rightarrow ^3\text{H}_4$  transition following a classical Beer-Lambert absorption law) and UC pumping (the ESA  $^3\text{F}_4 \rightarrow ^3\text{F}_{2,3}$  transition based on a photon avalanche effect), it is found that different focal lengths of the L<sub>1</sub> focusing lens lead to optimum laser performances in these two cases. Indeed, shorter focal length ( $f = 50$  mm) is preferable for pure UC pumping as it leads to higher incident pump intensity and, thus, stronger photon avalanche effect and higher pump absorption. In contrast, for pure direct pumping, an L<sub>1</sub> lens with  $f = 150$  mm provides better mode matching with a relatively good absorption efficiency since the absorption coefficient is independent of the pump intensity.

First, we study single-wavelength UC pumping. As explained above, an L<sub>1</sub> lens with a focal length of  $f = 50$  mm is used, Fig. 4(a). Pumping at  $\lambda_{\text{p,UC}} = 1.05$  μm (the  $^3\text{F}_4 \rightarrow ^3\text{F}_{2,3}$  ESA transition), the output power of the MIR Tm-laser reaches 110 mW at 2.31 μm with a slope efficiency  $\eta$  of 7.6% (vs. the incident pump power  $P_{1.05\mu\text{m}}$ ) and a laser threshold of 0.51 W. However, the slope efficiency vs. the absorbed pump power is relatively high, 29%, which then rises the interest of using the Yb-laser technology for pumping Tm<sup>3+</sup>-doped materials emitting at 2.3 μm. A typical spectrum of the laser emission is shown in Fig. 4(b). The laser emitted linearly polarized radiation ( $\pi$ ) and its polarization state is naturally selected by the anisotropy of the gain medium. To illustrate the superiority of the short focal length L<sub>1</sub> lens for pure UC pumping, both the input-output dependences of the Tm-laser for  $f = 50$  mm and  $f = 150$  mm are given in Fig. 4(a). Using the latter lens, the maximum output power of the MIR Tm-laser was only 80 mW corresponding to an increased threshold of 1.2 W.

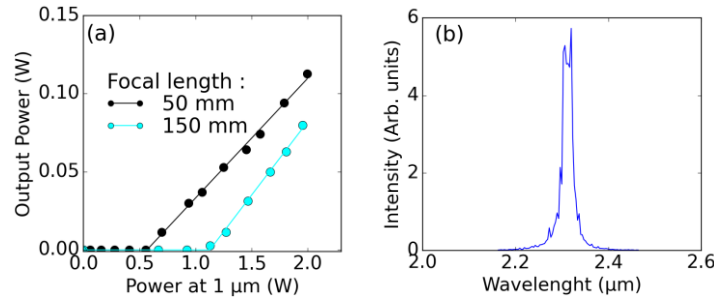


**Fig. 4.** Tm:LiYF<sub>4</sub> laser emitting at 2.3 μm with pure UC pumping by an Yb:CaF<sub>2</sub> laser emitting at 1050 nm: (a) input-output dependences for different focal lengths of the focusing lens (L<sub>1</sub>):  $f = 50$  mm and  $f = 150$  mm; (b) a typical spectrum of laser emission.

The dual-wavelength pumping is studied by fixing the power level of one pump source and

varying that of the second one. The laser output powers are plotted versus the total incident pump power,  $P_{\Sigma} = P_{0.78\mu\text{m}} + P_{1.05\mu\text{m}}$  and the slope efficiency and the laser threshold are determined with respect to  $P_{\Sigma}$  – for fair comparison. To assist UC pumping, the  $P_{0.78\mu\text{m}}$  value is fixed at several different levels and  $P_{1.05\mu\text{m}}$  is varied, as shown in Fig. 5(a). With increasing the added  $P_{0.78\mu\text{m}}$  power up to 2.0 W, both the maximum output power of the Tm-laser and its slope efficiency  $\eta$  gradually increase reaching 500 mW and 15.0%, respectively, Fig. 5(a,b).

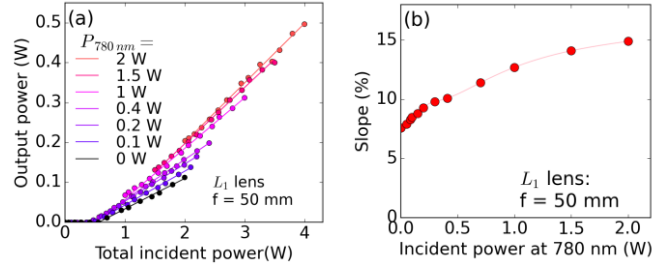


**Fig. 5.** Dual-wavelength-pumped MIR Tm:LiYF<sub>4</sub> laser,  $P_{0.78\mu\text{m}}$  – fixed,  $P_{1.05\mu\text{m}}$  – varied: (a) input-output dependences,  $L_1$  focusing lens:  $f = 50\text{ mm}$ ; (b) laser slope efficiencies vs. the total incident pump power ( $P_{\Sigma}$ ) plotted against the added  $P_{0.78\mu\text{m}}$  pump power

In all the experiments, the Tm-laser operates solely on the  $^3\text{H}_4 \rightarrow ^3\text{H}_5$  transition and no laser at  $1.9\mu\text{m}$  is observed.

For completeness, we have also studied pure direct pumping using an  $L_1$  lens with a focal length  $f = 150\text{ mm}$ . As the goal of the present work is the observation of the mutual interplay between the two pumps, the laser cavity and the pump focusing optics are not separately optimized for direct pumping as in the previous studies [10,11]. Pumping at  $\lambda_{\text{P,GSA}} = 0.78\mu\text{m}$  (the  $^3\text{H}_6 \rightarrow ^3\text{H}_4$  GSA transition), the MIR Tm-laser generates a maximum output power of 480 mW at  $2.31\mu\text{m}$  with a slope efficiency  $\eta$  of 20.9% (vs. the incident pump power  $P_{0.78\mu\text{m}}$ ) and a laser threshold of 0.47 W, Fig. 6(a). Then, we have again implemented dual-wavelength pumping: the added  $P_{1.05\mu\text{m}}$  pump power is fixed at different levels and  $P_{0.78\mu\text{m}}$  varies, Fig. 6(a). With a maximum added  $P_{1.05\mu\text{m}}$  pump power of 0.86 W, the maximum output power of the Tm-laser increases to 664 mW, its slope efficiency  $\eta$  increases to 24.5%, whilst the laser threshold also increases up to 0.85 W, Fig. 6(b). In this way, an addition of a small fraction of upconversion pump to the direct one has much weaker effect on the laser performance.

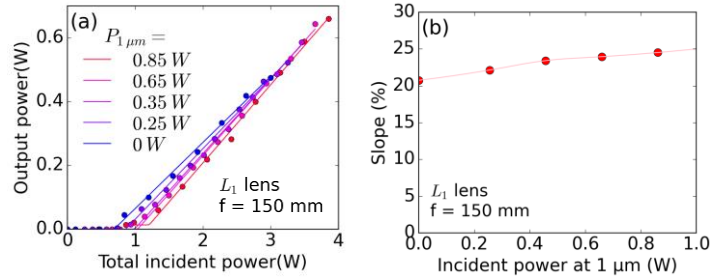


**Fig. 6.** Dual-wavelength-pumped MIR Tm:LiYF<sub>4</sub> laser:  $P_{0.78\mu\text{m}}$  – varied,  $P_{1.05\mu\text{m}}$  – fixed: (a) input-output dependences; (b) the corresponding laser slope efficiencies plotted against the added  $P_{1.05\mu\text{m}}$  pump power.  $L_1$  lens:  $f = 150\text{ mm}$ .

Let us discuss the observed laser behavior. The pumping at  $0.78\mu\text{m}$  leads to a direct excitation of  $\text{Tm}^{3+}$  ions to the upper laser level ( $^3\text{F}_4$ ). It can result in an emission of a laser photon at  $2.3\mu\text{m}$  followed by a non-radiative (NR) relaxation step to the intermediate



metastable level  $^3F_4$  or in its population via the CR process for adjacent  $Tm^{3+}$  ions,  $^3H_4 + ^3H_6 \rightarrow ^3F_4 + ^3F_4$ . Thus, for direct pumping, the metastable  $^3F_4$   $Tm^{3+}$  state accumulates the electronic excitations. The UC pumping at  $1.05 \mu m$  is based on a weak (non-resonant) GSA,  $^3H_6 \rightarrow ^3H_5$ , followed by a NR relaxation step to the  $^3F_4$  state, and a resonant ESA,  $^3F_4 \rightarrow ^3F_{2,3}$ , again followed by a NR relaxation step terminating at the upper laser level,  $^3H_4$ . For low incident pump intensities, the ESA process is very weak because of the non-resonant GSA channel and, thus, negligible population of the metastable  $^3F_4$  state. With increasing the incident pump intensity at  $1.05 \mu m$ , both the  $^3H_4$  and  $^3F_4$  states accumulate electronic excitations owing to the photon avalanche mechanism based on a combination of the ESA and CR.

The population of the metastable  $^3F_4$  state is crucial for boosting the efficiency of the ESA process  $^3F_4 \rightarrow ^3F_{2,3}$  which is a prerequisite for efficient laser operation under pure UC pumping and the population of this state could be easily increased by direct pumping representing a *seeding* effect on the UC pump absorption. It is indeed priming the UC pumping. Thus, dual-wavelength pumping relying mainly on the UC pump with a small addition of the direct pump could lead to reduced laser thresholds and boosted laser efficiencies of MIR Tm-lasers as compared to the case of pure UC pumping.

To illustrate this, we have plotted the measured laser thresholds of the dual-wavelength-pumped Tm laser for different combinations of the incident pump powers  $P_{0.78\mu m}$  and  $P_{1.05\mu m}$ , Fig. 7. The  $L_1$  lens with a focal length of 50 mm was chosen as it corresponded to the best performance in the case of pure UC pumping. In Fig. 7, each point represents a threshold pump power,  $P_{th} = P_{0.78\mu m} + P_{1.05\mu m}$ , then showing a combination of both pumps needed to reach the laser threshold. The intersections of this curve with the horizontal and vertical axes represent the two extreme cases of single-wavelength pumping: pure direct pumping with  $\lambda_{p,GSA} = 0.78 \mu m$  on the abscise axis, and pure UC pumping with  $\lambda_{p,UC} = 1.05 \mu m$  on the ordinate axis, respectively. Compared to single-wavelength UC-pumping, an addition of even a small contribution of the direct pump ( $P_{0.78\mu m} < 0.2$  W) helps to notably reduce the laser threshold in terms of the total pump power. This is due to the seeding effect of the direct pump on the population of the intermediate  $^3F_4$  state as explained above. To highlight this effect, we also plotted the isopower lines in order to clearly see that this process is more pronounced for a small fraction of the direct pump revealing then a seeding effect.

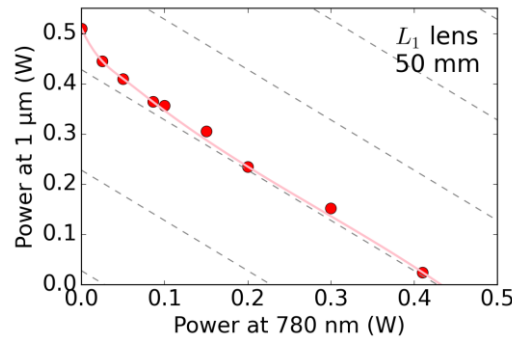


**Fig. 7.** Analysis of the threshold behavior of the dual-wavelength pumped MIR Tm:LiYF<sub>4</sub> laser: thresholds for different combinations of the incident pump powers  $P_{0.78\mu m}$  and  $P_{1.05\mu m}$ . Grey lines – isopower lines drawn as guides for eyes.

Another way to express the seeding effect of the added direct pump is to monitor the output power of the MIR Tm-laser as a function of the ratio between the added  $P_{0.78\mu m}$  power and the total incident pump power  $P_{\Sigma}$ , namely  $X = P_{0.78\mu m}/P_{\Sigma}$ . Figure 8 illustrates such analysis for a fixed value of  $P_{\Sigma} = 2.0$  W and for a focal length for  $L_1$  of  $f = 50$  mm. Here, the cases of  $X = 0$  and  $X = 1$  correspond to pure UC pumping and pure direct pumping, respectively. As can be seen from Fig. 8, the main effect of adding the direct pump on the output power is observed for small  $X$  values and for  $X > 0.5$ , the dependence saturates, therefore indicating an area of interest



270 towards lower  $X$  values.

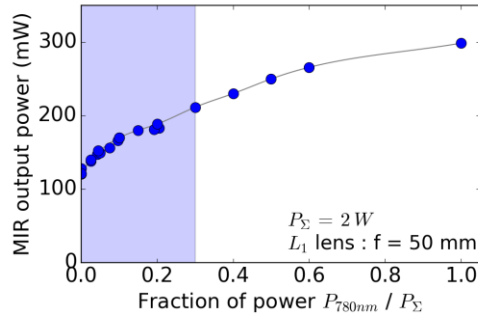


**Fig. 8.** Output power of the dual-wavelength pumped MIR Tm:LiYF<sub>4</sub> laser as a function of the fraction of the direct pump to the total incident pump power,  $P_{0.78\mu\text{m}}/P_{\Sigma}$ .  $P_{\Sigma} = 2.0$  W,  $L_1$  lens:  $f = 50$  mm. *Blue rectangle:* the zone of interest.

We have studied the total pump absorption in the Tm:LiYF<sub>4</sub> crystal at both wavelengths (0.78  $\mu\text{m}$  and 1.05  $\mu\text{m}$ ) under single- and dual-wavelength pumping and non-lasing conditions, Fig. 9. To assist UC pumping, the added  $P_{0.78\mu\text{m}}$  power is fixed at several different levels and  $P_{1.05\mu\text{m}}$  varies. For this experiment, the focusing lens  $L_1$  with a focal length of  $f = 50$  mm is selected. One can then observe a strong effect of the dual-wavelength pumping on the pump absorption. This effect is also more impacting at lower level of  $\lambda_{\text{P,GSA}} = 0.78$   $\mu\text{m}$

For pure UC pumping, Fig. 9(a), the pump absorption at 1.05  $\mu\text{m}$  increases with the incident pump power and saturates at  $\sim 34\%$  for  $P_{1.05\mu\text{m}} > 0.4$  W. By adding more pump at 0.78  $\mu\text{m}$ , this tendency changes first to almost pump-independent absorption (at  $P_{0.78\mu\text{m}} = 0.19$  W) and then it is even reversed representing an absorption saturation effect. The saturated pump absorption slightly increases with the added  $P_{0.78\mu\text{m}}$  power, from 34% to 40%, as shown in Fig. 9(a), representing a positive effect of the dual-wavelength pumping. These observations are in line with the laser behavior, and they are explained by the increased population of the metastable  $^3\text{F}_4$  state acting as an “effective” ground-state for the  $^3\text{F}_4 \rightarrow ^3\text{F}_{2,3}$  ESA channel. It is for the first time that we observe a *recycling* process of the population of the metastable  $^3\text{F}_4$  state by ESA in the  $^3\text{F}_4 \rightarrow ^3\text{F}_{2,3}$  loop favoring the 2.3  $\mu\text{m}$  laser. Despite the fact that the measurements are performed under non-lasing conditions, as the main effect of the dual-wavelength pumping on the pump absorption is observed below the laser threshold, so that the obtained conclusions held true for the lasing regime as well.

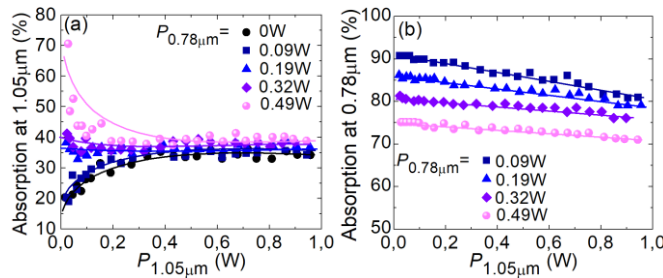


**Fig. 9.** Total pump absorption for a dual-wavelength-pumped MIR Tm:LiYF<sub>4</sub> laser under non-lasing conditions measured at: (a)  $\lambda_{\text{P,UC}} = 1.05$   $\mu\text{m}$ , (b)  $\lambda_{\text{P,GSA}} = 0.78$   $\mu\text{m}$ ,  $P_{0.78\mu\text{m}} = \text{fixed}$ ,  $P_{1.05\mu\text{m}} = \text{varied}$ .  $L_1$  lens,  $f = 50$  mm.

A very different behavior is observed for the pump absorption at 0.78  $\mu\text{m}$ . With increasing the pump power at 1.05  $\mu\text{m}$ , it decreases marginally due to a slight decrease of the ground-state population since a part of the  $^3\text{F}_4$  population is directly recycled in the upper loop instead of fluorescing back to the ground level. This recycling effect explains the increase of the laser

power and slope efficiency, Fig. 6(b), when using dual-pumping despite a lower absorption at 0.78  $\mu\text{m}$ , cf. Fig. 9(b).

The observed rapid increase of the pump absorption at 1.05  $\mu\text{m}$  under co-pumping at 0.78  $\mu\text{m}$  (even for relatively low added pump powers) is responsible for the useful decrease of the laser threshold of the dual-wavelength-pumped Tm:LiYF<sub>4</sub> laser, cf. Fig. 7. It is also partially responsible of the increase of the laser slope efficiency, as shown in Fig. 5(b). Another possible reason is the nonlinearity of the input-output dependences of Tm lasers operating on the  $^3\text{H}_4 \rightarrow ^3\text{H}_5$  transition [12] due to the enhanced effect of ETU from the metastable  $^3\text{F}_4$  state refilling the upper laser level.

#### 4. Conclusion

To conclude, we have studied in detail the dual-wavelength (combining direct and upconversion) pumping of a Tm:LiYF<sub>4</sub> laser operating on the  $^3\text{H}_4 \rightarrow ^3\text{H}_5$  transition corresponding to an emission in the MIR, at 2.3  $\mu\text{m}$ . As an UC pump source, we used a Yb:CaF<sub>2</sub> laser tuned to one of the ESA ( $^3\text{F}_4 \rightarrow ^3\text{F}_{2,3}$ ) peaks of Tm<sup>3+</sup> ions at 1.05  $\mu\text{m}$ . Such fine matching of the ESA peak was critical to reach a reasonably high pump absorption via the photon avalanche mechanism. This particular matching between the Yb:CaF<sub>2</sub> pump and Tm:YLF laser technologies was experimentally demonstrated for the first time, in our best knowledge. For pure UC pumping, the MIR Tm laser delivered 110 mW at 2.31  $\mu\text{m}$  for 2.0 W of incident pump power corresponding to a slope efficiencies of 7.6% and 29% versus the incident and absorbed pump power, respectively. Furthermore, we found that the co-pumping at 0.78  $\mu\text{m}$  helps to notably reduce the laser threshold due to the seeding effect on the population of the intermediate  $^3\text{F}_4$  Tm<sup>3+</sup> state. We also observed a recycling process of this long-lifetime-manifold population by resonant ESA that goes in favour of the 2.3  $\mu\text{m}$  laser. Considering the availability of high-power and high-brightness pump sources at 1  $\mu\text{m}$  based on the Yb-fiber laser technology, and low- to moderate-power single-mode fiber-coupled 0.8  $\mu\text{m}$  AlGaAs laser diodes, a combination of these two pump sources could serve as a viable way for the development of MIR Tm lasers, especially those for which a high-brightness pumping and / or a compatibility with the fiber laser technology are required, such as fiber and waveguide lasers and bulk femtosecond oscillators and amplifiers. This is especially relevant for the latter type of laser sources which are currently pumped by tunable Ti:Sapphire lasers thus strongly limiting their applications.

**Funding.** Agence Nationale de la Recherche (ANR-19-CE08-0028, SPLENDID2). “RELANCE” Chair of Excellence project funded by the Normandy Region.

**Disclosures.** The authors declare no conflicts of interest.

**Data availability.** Data underlying the results presented in this paper are not publicly available at this time but may be obtained from the authors upon reasonable request.

#### References

1. F. J. McAleavey, J. O’Gorman, J. F. Donegan, B. D. MacCraith, J. Hegarty and G. Maze, “Narrow linewidth, tunable Tm<sup>3+</sup>-doped fluoride fiber laser for optical-based hydrocarbon gas sensing,” *IEEE J. Sel. Top. Quantum Electron.* **3**(4), 1103-1111 (1997).
2. G. G. Taylor, D. Morozov, N. R. Gemmell, K. Erotokritou, S. Miki, H. Terai, and R. H. Hadfield, “Photon counting LIDAR at 2.3  $\mu\text{m}$  wavelength with superconducting nanowires,” *Opt. Express* **27**(26), 38147-38158 (2019).
3. V. Petrov, “Frequency down-conversion of solid-state laser sources to the mid-infrared spectral range using non-oxide nonlinear crystals,” *Progr. Quantum Electron.* **42**, 1–106 (2015).
4. I. Moskalev, S. Mirov, M. Mirov, S. Vasilyev, V. Smolski, A. Zakrevskiy, and V. Gapontsev, “Ultrafast middle-IR lasers and amplifiers based on polycrystalline Cr:ZnS and Cr:ZnSe,” *Opt. Mater. Express* **7**(7), 2636-2650 (2017).
5. E. Geerlings, M. Rattunde, J. Schmitz, G. Kaufel, H. Zappe, and J. Wagner, “Widely tunable GaSb-based external cavity diode laser emitting around 2.3  $\mu\text{m}$ ,” *IEEE Photon. Technol. Lett.* **18**(18), 1913-1915 (2006).
6. U. Sheintop, D. Sebbag, P. Komm, S. Pearl, G. Marcus, and S. Noach, “Two-wavelength Tm:YLF/KGW external-cavity Raman laser at 2197 nm and 2263 nm,” *Opt. Express* **27**(12), 17112-17121 (2019).

- 353 7. J. Caird, L. DeShazer, and J. Nella, "Characteristics of room-temperature 2.3- $\mu\text{m}$  laser emission from  $\text{Tm}^{3+}$  in  
354 YAG and  $\text{YAlO}_3$ ," IEEE J. Quantum Electron. **11**(11), 874-881 (1975).
- 355 8. J. F. Pinto, L. Esterowitz, and G. H. Rosenblatt, " $\text{Tm}^{3+}$ :YLF laser continuously tunable between 2.20 and 2.46  
356  $\mu\text{m}$ ," Opt. Lett. **19**(12), 883-885 (1994).
- 357 9. E. Kifle, P. Loiko, L. Guillemot, J.-L. Doualan, F. Starecki, A. Braud, T. Georges, J. Rouvillain, and P. Camy,  
358 "Watt-level diode-pumped thulium lasers around 2.3  $\mu\text{m}$ ," Appl. Opt. **59**(25), 7530-7539 (2020).
- 359 10. P. Loiko, R. Soulard, L. Guillemot, G. Brasse, J.-L. Doualan, A. Braud, A. Tyazhev, A. Hideur, B. Guichardaz,  
360 F. Druon, and P. Camy, "Efficient  $\text{Tm}:\text{LiYF}_4$  lasers at  $\sim 2.3$   $\mu\text{m}$ : Effect of energy-transfer upconversion," IEEE  
361 J. Quantum Electron. **55**(6), 1700212 (2019).
- 362 11. I. Yorulmaz and A. Sennaroglu, "Low-threshold diode-pumped 2.3- $\mu\text{m}$   $\text{Tm}^{3+}$ :YLF lasers," IEEE J. Sel. Top.  
363 Quantum Electron. **24**(5), 1601007-1-7 (2018).
- 364 12. L. Guillemot, P. Loiko, R. Soulard, A. Braud, J.-L. Doualan, A. Hideur, and P. Camy, "Close look on cubic  
365  $\text{Tm}:\text{KY}_3\text{F}_{10}$  crystal for highly efficient lasing on the  $^3\text{H}_4 \rightarrow ^3\text{H}_5$  transition," Opt. Express **28**(3), 3451-3463  
366 (2020).
- 367 13. P. Loiko, E. Kifle, L. Guillemot, J.-L. Doualan, F. Starecki, A. Braud, M. Aguiló, F. Díaz, V. Petrov, X.  
368 Mateos, and P. Camy, "Highly efficient 2.3  $\mu\text{m}$  thulium lasers based on a high-phonon-energy crystal: evidence  
369 of vibronic-assisted emissions," J. Opt. Soc. Am. B **38**(2), 482-495 (2021).
- 370 14. L. Guillemot, P. Loiko, A. Braud, J.-L. Doualan, A. Hideur, M. Koselja, R. Moncorge, and P. Camy,  
371 "Continuous-wave  $\text{Tm}:\text{YAlO}_3$  laser at  $\sim 2.3$   $\mu\text{m}$ ," Opt. Lett. **44**(20), 5077-5080 (2019).
- 372 15. R. Soulard, A. Tyazhev, J.L. Doualan, A. Braud, A. Hideur, M. Laroche, B. Xu, and P. Camy, "2.3  $\mu\text{m}$   
373  $\text{Tm}^{3+}$ :YLF mode-locked laser," Opt. Lett. **42**(18), 3534-3536 (2017).
- 374 16. F. Canbaz, I. Yorulmaz, and A. Sennaroglu, "Kerr-lens mode-locked 2.3- $\mu\text{m}$   $\text{Tm}^{3+}$ :YLF laser as a source of  
375 femtosecond pulses in the mid-infrared," Opt. Lett. **42**(19), 3964-3967 (2017).
- 376 17. L. Guillemot, P. Loiko, R. Soulard, A. Braud, J.-L. Doualan, A. Hideur, R. Moncorgé, and P. Camy, "Thulium  
377 laser at  $\sim 2.3$   $\mu\text{m}$  based on upconversion pumping," Opt. Lett. **44**(16), 4071-4074 (2019).
- 378 18. Y. Morova, M. Tonelli, V. Petrov, and A. Sennaroglu, "Upconversion pumping of a 2.3  $\mu\text{m}$   $\text{Tm}^{3+}:\text{KY}_3\text{F}_{10}$  laser  
379 with a 1064 nm ytterbium fiber laser," Opt. Lett. **45**(4), 931-934 (2020).
- 380 19. M. F. Joubert, S. Guy, and B. Jacquier, "Model of the photon-avalanche effect," Phys. Rev. B **48**(14), 10031-  
381 10037 (1993).
- 382 20. A. Tyazhev, F. Starecki, S. Cozic, P. Loiko, L. Guillemot, A. Braud, F. Joulain, M. Tang, T. Godin, A. Hideur,  
383 and P. Camy, "Watt-level efficient 2.3  $\mu\text{m}$  thulium fluoride fiber laser," Opt. Lett. **45**(20), 5788-5791 (2020).
- 384 21. F. Wang, H. Huang, H. Chen, Y. Bao, Z. Li, and D. Shen, "GSA and ESA dual-wavelength pumped 2.3  $\mu\text{m}$   
385  $\text{Tm}:\text{YLF}$  laser on the  $^3\text{H}_4 \rightarrow ^3\text{H}_5$  transition," Chin. Opt. Lett. **19**(9), 091405 (2021).